Supporting information for

Quantum Rate Dynamics and Charge Screening at the Nanoscale Level

Edgar Fabian Pinzón Nieto,[a] Erika Viviana Godoy Alarcón,[a] Yuliana Pérez Sánchez,[a] and Paulo Roberto Bueno[a*]

[a]Institute of Chemistry, São Paulo State University (UNESP), 14800-900, Araraquara, São Paulo, Brazil

*Corresponding author: paulo-roberto.bueno@unesp.br

SI.1. Fabrication process and characterization of molecular and nanoscale semiconducting films

In this section, additional details about the fabrication process and chemical characterization of two nanoscale junctions (redox peptide monolayers and Cu_2O/CuO mixed nanofilms), on which it was carried out the quantum rate analysis, are presented. As demonstrated in the main text, although these junctions have different chemical nature (organic and inorganic) and electronic occupancy (redox and non-redox), the charging state dynamics obeys a common quantum electrochemical screening (QES) concept.

Peptide characterization

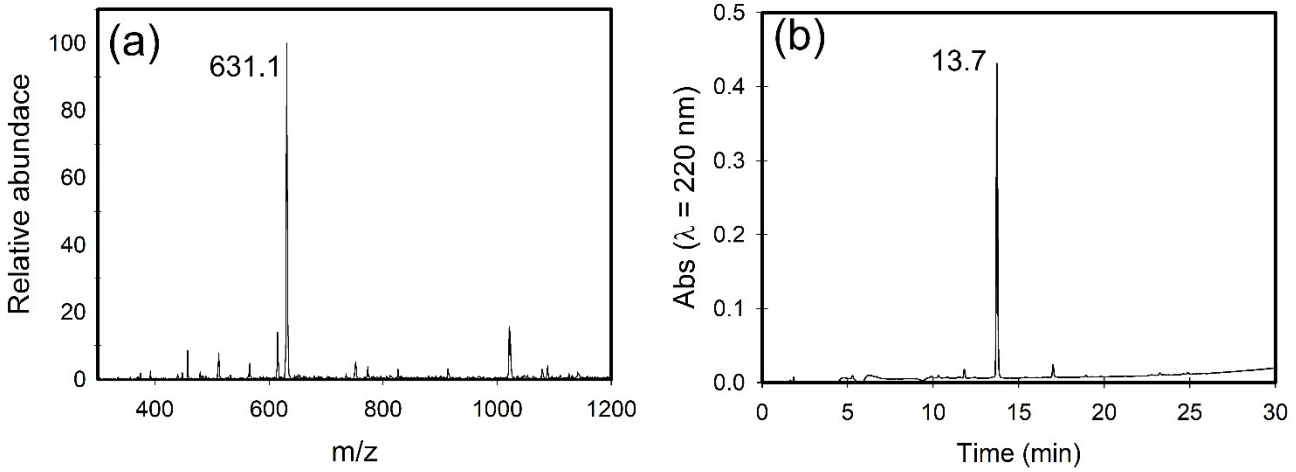

Figure SI.1. (a) Mass spectrum of the ferrocene-peptide that was acquired using a Brucker mass spec system in positive mode, m/z = 631.15 g mol^{-1}, corresponding to the peak of 13.7 min in (b). (b) Chromatogram of the purified ferrocene-peptide (i.e., purity > 96%) with retention time of 13.7 min.

Fabrication of the nanoscale copper oxide mixed films

Fabrication and electrochemical methods summarized here are complementary reported elsewhere.[1] The assembly and electrochemical characterization of copper oxide films were carried

out in a three-electrode conventional setup where a gold electrode served as working electrode, AglAgCl (3 M KCl) as reference and a platinum mesh was employed as counter electrode. The copper electrodeposition conditions were chosen from studies of electrochemical behavior of Cu^{2+} on gold electrodes. Figure SI.2 shows a cyclic voltammogram (CV) obtained for 0.01 Cu^{2+} in acid medium in which two reduction peaks were identified. Starting from the cathodic direction, the C_1 peak is associated to the deposition of an atomic copper layer which is known to occurs in underpotential conditions that follows Eq. S1.[2] At higher potentials, the peak C_2 corresponds to the bulk or to overpotential deposition of copper described by Eq. S2.[3] Finally, the inverse potential scan showed A_1 and A_2 anodic peaks associated to the stripping of deposited copper in C_1 and C_2 peaks, respectively.

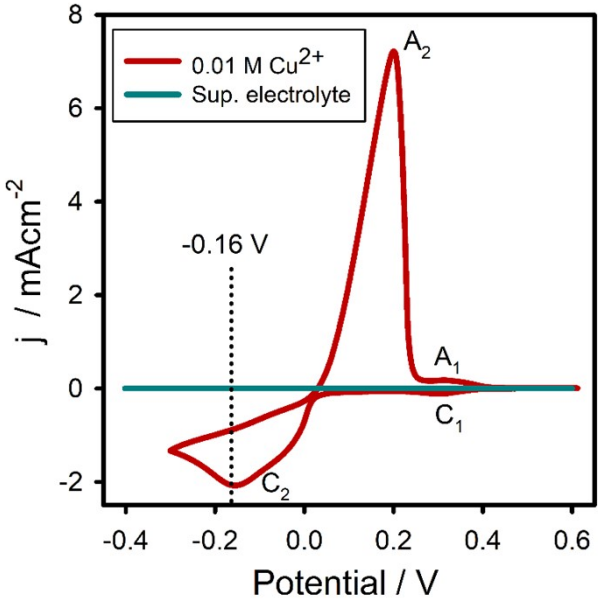

Figure SI.2. Cyclic voltammogram obtained on a polycrystalline gold electrode from an oxygen-free acid solution containing 0.01 M $CuSO_4$ in 0.02 M H_2SO_4.

$$Cu^{2+} + 2e^- \leftrightharpoons Cu^0_{Sub} \quad \text{(S1)}$$

$$Cu^{2+} + 2e^- \leftrightharpoons Cu^0_{Over} \quad \text{(S2)}$$

In order to obtain a copper thin film thicker than an atomic monolayer, the value of -0.16 V was chosen as the deposition potential because of its location at overpotential region of deposition and slightly to the higher C_2 peak potential which guarantee the diffusion-controlled deposition of copper (see Figure SI.2).[4] Copper thin films of different thicknesses were deposited by applying a constant potential of -0.16 V on gold electrodes by 30, 60, 90, 180 and 300 s. The transient of electric current obtained from above potentiostatic deposition procedure is presented in Figure SI.3. The film thicknesses were estimated electrochemically using Faraday's law according to Eq. S3, where d is the thickness of deposited material, Q the charge, M the molecular weight of the copper, F the Faraday's constant, z the number of electrons involved in the electrochemical process, ρ the density of the cooper and A the electroactive area.[5] Q was calculated from the

integration of the current transients recorded for each deposition time. The estimated thicknesses are presented in Table SI.1 where values from 5.8 to 35.0 nm were obtained for deposition times between 30 and 300 s.

$$d = \frac{Q\,M}{F\,z\,\rho\,A} \qquad \text{(S3)}$$

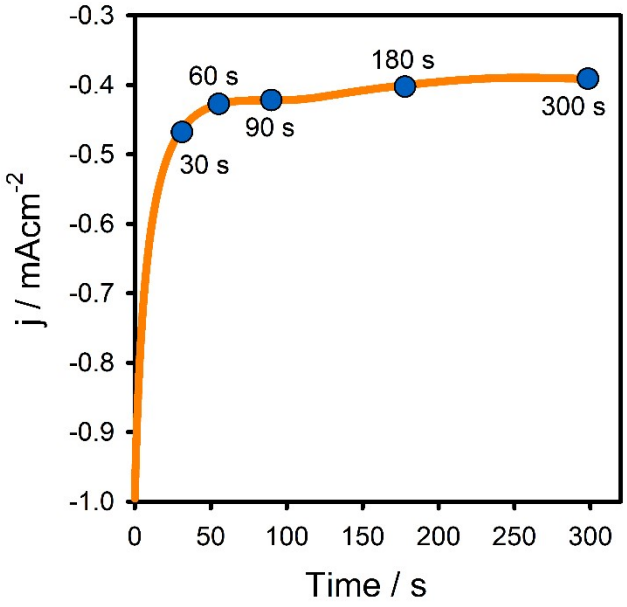

Figure SI.3. Electric current transient for a polycrystalline gold electrode obtained by applying a constant potential pulse of -0.16 V in an oxygen-free solution containing 0.01 M $CuSO_4$ in 0.02 M H_2SO_4.

Table SI.1. Estimated thicknesses of the copper thin films obtained for different deposition times.

Deposition time (s)	Thickness (nm)
30	5.8
60	8.5
90	12.0
180	20.0
300	35.0

Subsequently, the oxidation behavior of the copper thin films was studied in 1 M NaOH by cyclic voltammetry. Figure SI.4a shows the CVs copper films showing three anodic peaks. Starting from the anodic direction, the A_1 peak corresponds to the oxidation of the surface where metal copper was converted to cuprous oxide (Cu_2O). The A_2 peak is associated to the oxidation of Cu_2O to cupric oxide (CuO). Finally, the A_3 peak corresponded to the direct oxidation of metal copper to CuO. The above oxidation reactions are described by Eqs. S4 to S6.[6, 7]

$$2Cu + 2OH^- \rightleftarrows Cu_2O + H_2O + 2e^- \qquad \text{(S4)}$$

$$Cu_2O + 2OH^- \rightleftarrows 2CuO + H_2O + 2e^- \quad \text{(S5)}$$

$$Cu + 2OH^- \rightleftarrows CuO + H_2O + 2e^- \quad \text{(S6)}$$

C_1, C_2 and C_3 cathodic peaks corresponded to the reduction process associated to above-described anodic peaks. Accordingly, copper thin films were oxidized by performing a potential scan in the anodic direction, as showed in the linear scan voltammogram (LSV) of Figure SI.4b, where the composition of the copper oxide films was controlled. The stability of copper thin films under electrochemical oxidation was evaluated performing a potential scan from -0.60 to 0.35 V (complete oxidation). However, copper films with thickness lower than 12.0 nm (90 s) showed instability to the oxidation presenting a voltametric response distinct to that of Figure SI.4b. Hence, in order to guarantee the stability in the electrochemical oxidation, 180 s was chosen as a suitable deposition time for the deposition of copper films studied in this work. From the oxidation response showed in Figure SI.4b, three oxidation scans were defined to attain films with different compositions. All scans started at -0.60 V. The scan 1 up to -0.33 V generated only Cu_2O, the scan 2 up to -0.25 V led to a Cu_2O/CuO mixed film and the scan 3 up to 0.35 V assured the formation of solely CuO.

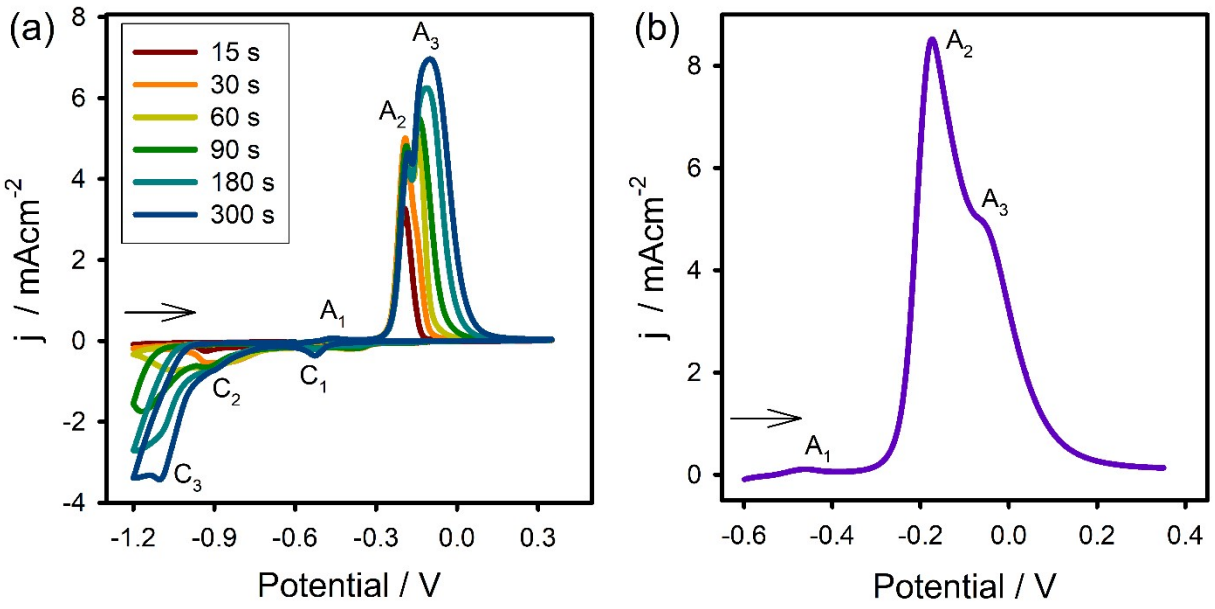

Figure SI.4. (a) Cyclic voltammograms and (b) linear sweep voltammogram for electrodeposited copper thin films at a scan rate of 60 mVs^{-1} in 1 M NaOH.

Characterization of the Copper Oxide nanoscale films

Estimation of the thickness

The thickness of copper oxide nanoscale films was electrochemically estimated using Eq. S3. The charge was determined through the mathematical integration of A_1, A_2 and A_3 anodic peaks identified in LSV of Figure SI.4b following

$$Q = \frac{1}{s}\int_{V_1}^{V_2} i(V)dV \quad , \qquad \text{(S7)}$$

where s is the scan rate, V_1 the initial potential, V_2 the final potential and i the oxidation current. However, as observed in Figure SI.4b, A_1, A_2, A_3 peaks (associated with oxidation reactions described by Eqs S4 to S6) presented an overlap between them which prevented the determination of the net charge contribution of each peak by a direct integration. To determine the net charge contribution associated to each oxidation process, a Gaussian deconvolution analysis was applied. As shown in Figure SI.5a, the A_1 peak (Figure SI.4b) was decomposed in three peaks whose cumulative sum (in gray) presented an accurate fitting to the experimental curve (in orange) (R^2 = 0.9982). The resultant peak 2, showed in the Figure SI.6a (in purple), was associated to the oxidation of Cu to Cu_2O. Moreover, the A_2 and A_3 peaks (Figure SI.3b) were decomposed into two peaks as observed in Figure SI.5b, whose cumulative sum also shows an accurate fitting (in gray) to the experimental curve (in orange) (R^2= 0.996). The discomposed peaks 4 and 5 associated with the

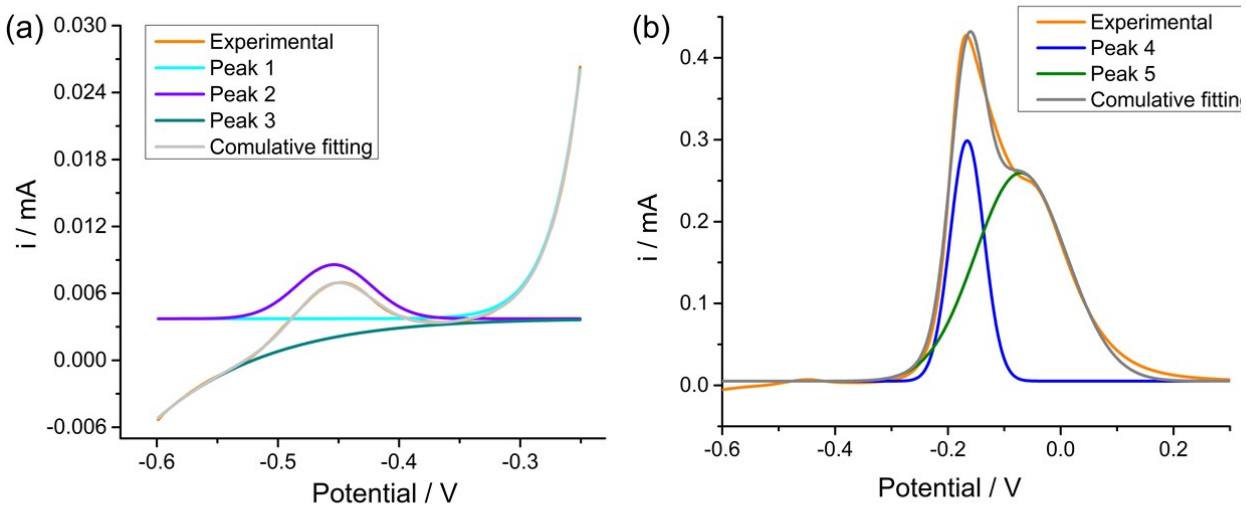

oxidation from Cu_2O to CuO and from Cu to CuO are shown in the Figure SI.6b and SI.6c, respectively.

Figure SI. 5. Gaussian deconvolution of the experimental oxidation peaks A_1 (a); A_2 and A_3 (b) observed for the Cu films in 1 M NaOH (Figure SI.4b).

Hence, the related charge Q for each oxidation scan was calculated by integrating the peaks resulting from the deconvolution analysis (Figure SI.6) and then applying Eq. S7. Considering a thin film configuration, the thickness of the Cu_2O (scan 1), Cu_2O/CuO (scan 2) and CuO (scan 3) nanofilms were estimated as the sum of the calculated thicknesses for each oxidation process from Eq. S14. The resultant thicknesses are presented in Table SI.2. The Cu_2O and Cu_2O/CuO compounds have an estimated thickness of 1.2 and 3.0 nm, while CuO compound have an estimated thickness of 20.0 nm.

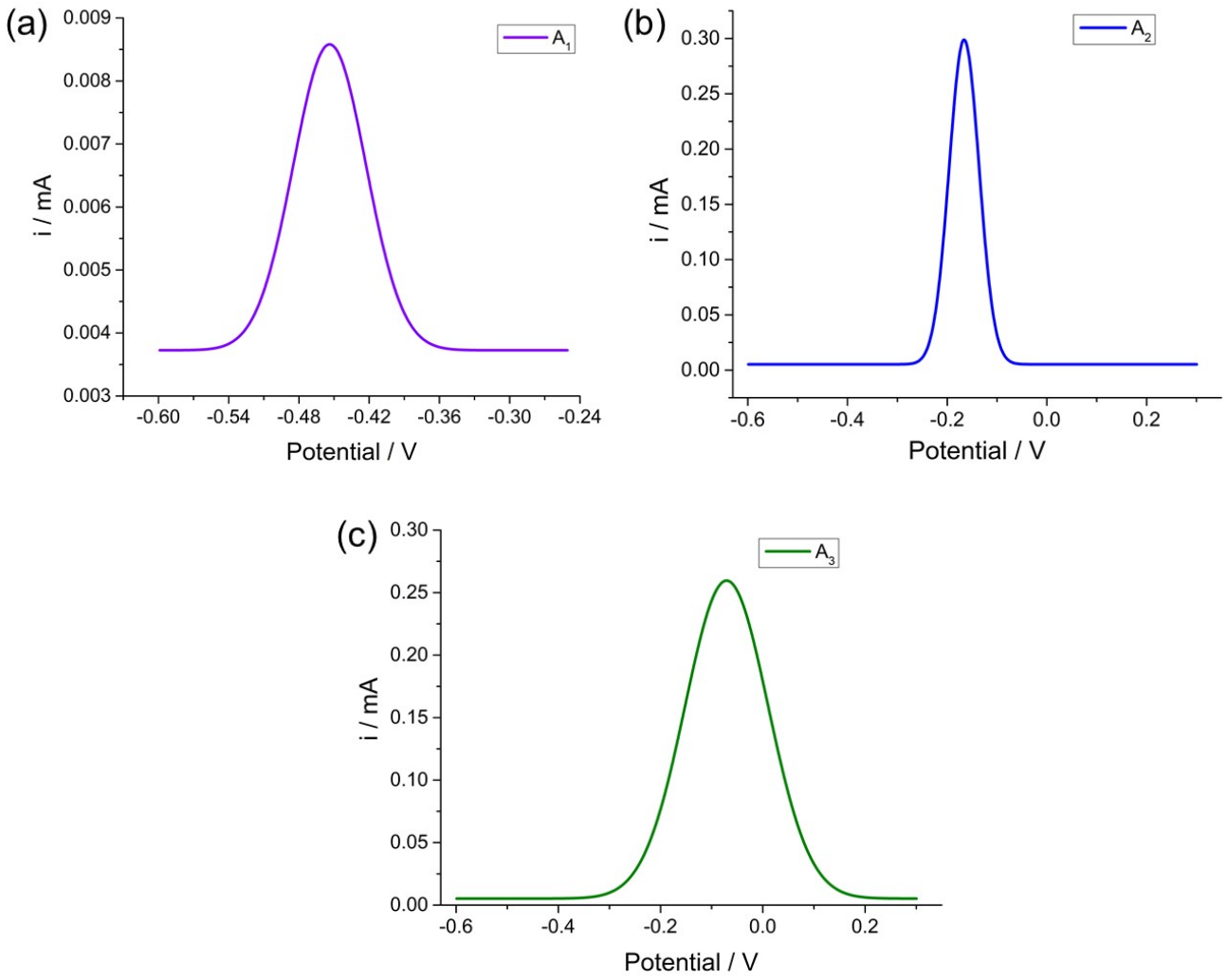

Figure SI.6. Peaks from a Gaussian deconvolution of oxidation peaks measured for the Cu films in 1 M NaOH. (a) The peak 2 associated with the oxidation of Cu to Cu_2O and peaks 4 (b) and 5 (c) associated with the oxidation of Cu_2O to CuO and of Cu to CuO, respectively.

Table SI.2. Estimated thicknesses for copper oxide thin films following Faraday's law (Eq. S3).

Oxidation scan	Composition	Thickness (nm)
1	Cu_2O	1.2
2	Cu_2O/CuO	3.0
3	CuO	20.0

Estimation of the ratio of Cu_2O to CuO in the copper oxide mixed nanoscale film

The ratio of Cu_2O to CuO in the Cu_2O/CuO films (oxidation scan 2) was estimated through the calculation of the ratio between the mass of the oxides electrochemically formed on the copper surface as presented in the previous section. The calculation of the masses was realized using the general expression of the Faraday's law given by:

$$m = \frac{Q\,M}{F\,z}, \qquad \text{(S8)}$$

where m corresponds to the mass of the material electrogenerated in the surface. Q involved in electrochemical oxidation was calculated using the same procedure described above. The calculated mass for Cu_2O and CuO are presented in Table SI.3, where a ratio of about 0.91 was obtained. The result indicated the presence of a copper oxide mixed condition of about 1:1 ratio of Cu_2O to CuO.

Table SI.3. Estimated Cu_2O/CuO ratio (1:1, w/w) using the Faraday´s law of electrolysis (Eq. S8).

Material	Mass (ng)
Cu_2O	4.53
CuO	4.98

Surface morphological analysis of mixed nanoscale semiconductor

Scanning electronic microscopy (SEM) was used to probe the morphology of Cu_2O/CuO (1:1, w/w) mixed nanoscale compounds. Figure SI.7 shows SEM images obtained for a polycrystalline gold surface (a-c), a copper film electrodeposited on the gold surface (d-f) and a Cu_2O/CuO compound electrochemically growth on a copper surface (g-i) at three different magnifications (x25000, 50000 and 10000). These SEM images show evident morphological differences between the three samples, confirming the changes in the surface in each stage of electrochemical modification described above. The polycrystalline gold surface (Figure SI.7a-c) is smooth with a homogeneous distribution of particles, while the surface of the copper film (Figure SI.7d-f) is rough presenting a distribution of greater size and heterogeneous particles. Finally, Cu_2O/CuO nanoscale compound surface (Figure SI.7g-i) presents a non-homogeneous and irregular morphology which is different from the previously samples.

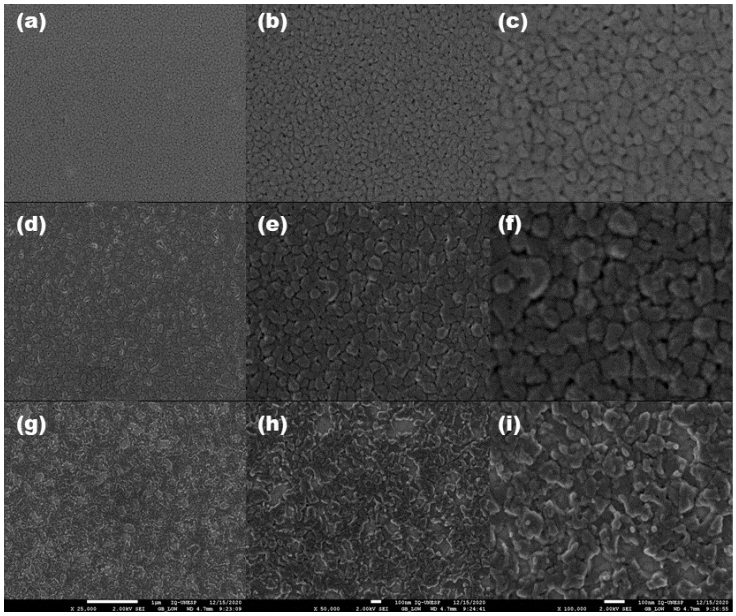

Figure SI.7. SEM images of the (a-c) polycrystalline gold surface, (d-f) copper film and (g-i) and the Cu_2O/CuO (1:1, w/w) mixed nanoscale compound at three magnifications (a-d-g) x25000, (b-e-h) x50000 and (c-f-i) x100000. Scanning Electron Microscope (TEM PHILIPS CM200) operated at 20.0 kV and 1.0000 nA was used to explore surface morphology.

SI.2. Electrochemical behavior of molecular and semiconductor interfaces

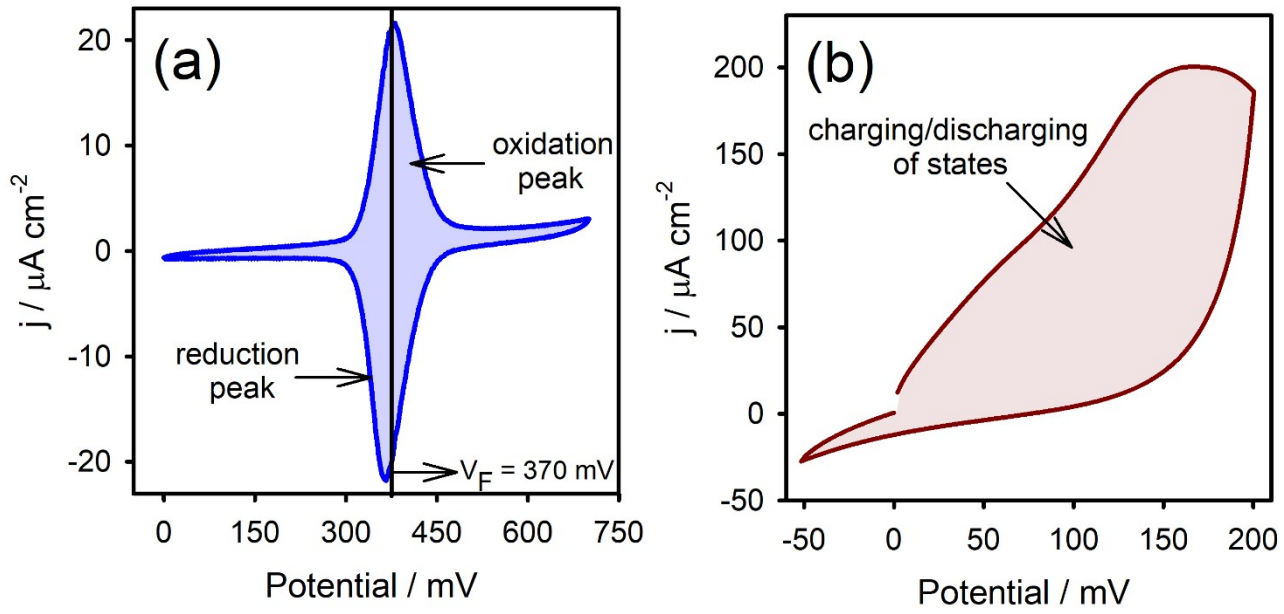

Figure SI.8. (a) Cyclic voltammogram of a Fc-pep monolayer, obtained at a scan rate of 0.1 Vs^{-1}, using 20 mM $TBAClO_4$ in ACN/H_2O (1:4 v/v) as supporting electrolyte. A symmetric Gaussian-like shape is observed for the anodic and cathodic processes following $Fc^+ + e^- \rightleftharpoons Fc$ reaction. (b) Cyclic voltammogram of Cu_2O/CuO nanofilms measured at 0.1 Vs^{-1} in PB solution (pH 7.4). The electrochemical profile of the oxide nanofilm presents the characteristic behavior of nanostructured semiconductor where there are no oxidation and reduction peaks as observed in the cyclic voltammogram. The current is associated to the occupation of electron states in the band gap and conduction band.[8]

SI. 3. Conductance calculations from the capacitive Nyquist plot

The conductance G function was calculated as $G = 2\pi f_r C''$, taking the maximum value of the imaginary capacitance C'' and its associated frequency (i.e., resonant frequency, f_r) from the capacitive Nyquist plot (see Figure SI.9), measured at each potential for the redox monolayer film and for semiconductor nanofilm.

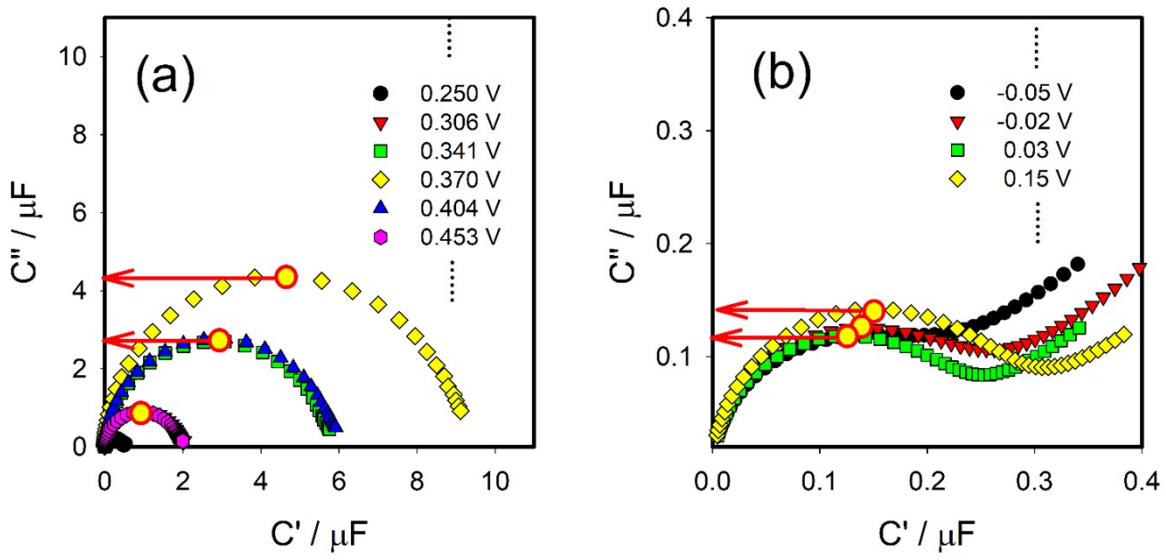

Figure SI.9. Capacitive Nyquist plot for (a) peptide monolayer and (b) Cu2O/CuO nanofilm. The arrows indicate the maximum values of C'' used to calculate G in order to obtain the molecular film conductance profile as $G = 2\pi f C''$.

SI.4. Capacitance at the molecular scale and frontier orbitals

As discussed in the main text there is a quantity $1/C_\mu$ defined as the series arrangement between electrostatic $1/C_e$ and quantum $1/C_q$ capacitances for charging molecular energy levels[9-11]. There are charging situations where $C_e \gg C_q$ and for this particular case the measured series and equivalent capacitance of molecular systems is quantized in nature[12] because $C_\mu \sim C_q$. For instance, this is the case for capacitively charged systems lower than 0.3 nm in the presence of an electrolyte. In the situations where $C_\mu \sim C_q$, the differential capacitance C_q can be defined and determined from the specific amount of work per unit of charge dV required to bring an amount of charge dq from the vacuum level to the molecular system in question such as $1/C_q = dV/dq$ and from an atomistic or molecular viewpoint C_q can be determined observing that[13]

$$edV = \mu(N + \Delta N) - \mu(N) \equiv d\mu \qquad \text{(S9)}$$

where $d\mu$ is the variation of the chemical potential μ of a system containing a determined number of electron particles N, referred as N-particle system; then by noting that $dq = edN$ and considering the variation of solely a particle, thus $dN = 1$ and the energy for this exchange of single electron particle is computed as

$$\frac{e^2}{C_q(N)} = \mu(N + \Delta N) - \mu(N) \qquad \text{(S10)}$$

and the chemical potential $\mu(N)$ can be defined as

$$\mu(N) = E(N) - E(N - 1) \qquad \text{(S11)}$$

and we can further note that this analysis can be related to the ionization potential and the electron affinity energies of the N-particle system such as

$$\mu(N) = E(N) - E(N-1) \tag{S12}$$

where $E(N)$ is the total energy and still it can be further noted that

$$I(N) = E(N-1) - E(N) \tag{S13}$$

and

$$A(N) = E(N) - E(N+1) \tag{S14}$$

are the ionization potential and the electron affinity of the N-particle system. Now it can be noted that the capacitance defined in Eq. (2) can be stated as[13, 14]

$$\frac{e^2}{C_q(N)} = I(N) - A(N) \tag{S15}$$

which can be connected with the quantum mechanical ionization potential and electron affinity by using conceptual Density Functional Theory (DFT) analysis where $I(N) - A(N)$ has been defined as the "absolute hardness" denoted as[15]

$$\eta = \frac{1}{2}[I - A] \tag{S16}$$

and is used in conjunction with[15]

$$\chi = \frac{1}{2}[I + A] \tag{S17}$$

where it can be noted that $\mu = -\chi$ from a conceptual Density Functional Theory (DFT) viewpoint. Finally, conceptual DFT review that

$$I(N) - A(N) = \epsilon(L) - \epsilon(H) + C \tag{S18}$$

where $\epsilon(L)$ and $\epsilon(H)$ are the lowest (LUMO) unoccupied and highest (HOMO) occupied molecular orbital energies as defined in DFT Kohm-Sham analysis and C is a constant. To summarize thus far, we can note that[16]

$$\frac{e^2}{C_q(N)} = \epsilon(L) - \epsilon(H) + C \tag{S19}$$

from which we can note that the quantum capacitance is directly associated with frontier orbitals of a molecular or with conduction (CB) and valence (VB) bands in semiconductive structures.

SI. 5. Analytical curves

Figure 3 of the main paper describes the analytical curves obtained for (a) NS1 protein detection (biomarker of dengue virus) and (b) phenol in solution using capacitive sensing platforms based on the redox peptide monolayers and Cu_2O/CuO nanoscale films, respectively. The relative response (RR %) in (a) versus the logarithm of NS1 concentration shows a linear tendency with a coefficient of determination R^2 = 0.9610. RR% was calculated as $\left[\left(\left({}^{1}/_{C_{q,n}} - {}^{1}/_{C_{q,0}}\right)/{}^{1}/_{C_{q,0}}\right)\right] \cdot 100$,

where $C_{q,0}$ is the capacitance response measured for an incubation in absence of the NS1 protein. The error bars in (a) represent the intraassay variability (standard error) between three consecutive measurements in the same sample. Note that (a) was adapted from reference [17]. RR% in (b) *versus* the logarithm of phenol concentration shows a linear tendency with R^2 = 0.9855. RR% was calculated as $\left[\left(\left(C_{q,n} - C_{q,0}\right)/C_{q,0}\right)\right] \cdot 100$, where $C_{q,0}$ is the capacitance response measured in a phosphate buffer solution (pH 7.4) in absence of phenol. The error bars in (b) represent the standard deviation between two independent interfaces as adapted from reference 1.

SI. 6. Calculation of specific capacitance

Peptide monolayer

The measured C_q of a redox molecular film at $V_F = e/E_F \sim 0.37\ V$ represents a maximum capacitance due to electron dynamic equilibrium $f = 1/2$, thus, $C_q = \left(e^2 N/k_B T\right)[f(1-f)] = e^2 N/4k_B T$, where N is the number of quantum channels (proportional to the number of redox-active molecules), thus calculated as $N = 4C_q k_B T/e^2$. In order to normalize the capacitance between the mass of the monolayer, one can take $m[g] = N\,M/N_A$, here N_A is the Avogadro´s constant and M is the molecular weight given by the mass spectrum (see Figure. SI.1b). This obtained mass was used to normalized the capacitance C_q measured at $V_F \sim 0.37\ V$ for four independent redox peptide interfaces, attaining an averaged value of $1493.15\ Fg^{-1}$ with a negligible standard deviation of $\sim 10^{-13}\ Fg^{-1}$.

Copper oxide mixed film

In order to obtain the value of C_q normalized between the mass of copper oxide at $V_F = e/E_F \sim -10\ mV$, corresponding to the Fermi level of semiconductor film. For $f = 1/2$, the total mass was calculated as the sum of the masses calculated in the section SI.4 (see Table SI.3). Hence, the value of C_q measured at $-10\ mV$ (not normalized by area) was divided by the total mass. This procedure was applied for three independent Cu_2O/CuO films leading to specific quantum capacitance value of $C_q = 27 \pm 2\ Fg^{-1}$.

References

1. E. F. Pinzón, A. d. Santos and P. R. Bueno, *ACS Applied Electronic Materials*, 2021, **3**, 3411-3417.
2. M. Yang, H. Zhang and Q. Deng, *Electrochemistry Communications*, 2017, **82**, 125-128.
3. K. Caban, *Journal of Solid State Electrochemistry*, 2009, **13**, 733-744.
4. C. Kartal, Y. Hanedar, T. Öznülüer and Ü. Demir, *Langmuir*, 2017, **33**, 3960-3967.
5. S. M. J. Zaidi, M. Z. Butt and F. Bashir, *Materials Research Express*, 2019, **6**, 046404.
6. Y. Wan, Y. Zhang, X. Wang and Q. Wang, *Electrochemistry Communications*, 2013, **36**, 99-102.
7. W. J. Stepniowski, S. Stojadinović, R. Vasilić, N. Tadić, K. Karczewski, S. T. Abrahami, J. G. Buijnsters and J. M. C. Mol, *Materials Letters*, 2017, **198**, 89-92.
8. J. Bisquert, F. Fabregat-Santiago, I. Mora-Seró, G. Garcia-Belmonte, E. M. Barea and E. Palomares, *Inorganica Chimica Acta*, 2008, **361**, 684-698.
9. P. R. Bueno, *Analytical Chemistry*, 2018, **90**, 7095-7106.

10. P. R. Bueno, *The Nanoscale Electrochemistry of Molecular Contacts*, Springer, 2018.
11. P. R. Bueno and J. J. Davis, *Chemical Society Reviews*, 2020, **49**, 7505-7515.
12. P. R. Bueno, *Journal of Power Sources*, 2019, **414**, 420-434.
13. G. J. Iafrate, K. Hess, J. B. Krieger and M. Macucci, *Physical Review B*, 1995, **52**, 10737-10739.
14. P. R. Bueno, G. T. Feliciano and J. J. Davis, *Physical Chemistry Chemical Physics*, 2015, **17**, 9375-9382.
15. R. G. Pearson, *Journal of Chemical Sciences*, 2005, **117**, 369-377.
16. J. P. Perdew, in *NATO Advanced Study Institute, Series B: Physics*, ed. R. M. Dreizler, Plenum, New York, 1985, vol. 123.
17. J. Cecchetto, A. Santos, A. Mondini, E. M. Cilli and P. R. Bueno, *Biosensors and Bioelectronics*, 2020, **151**, 111972.